applied optics

Optical bistability of partial reflection-coated thin film of oil red O

Quy Ho Quang,[1,2] Luu Mai Van,[3] Thanh Thai Doan,[1] Kien Bui Xuan,[4] Thang Nguyen Manh,[2] and Quang Ho Dinh[5,*]

[1]Ho Chi Minh City University of Food Industry, 140 Le Trong Tan Str., Tay Thanh Wart, Tan Phu Distr., Ho Chi Minh City, Vietnam
[2]Academy of Military Science and Technology, 17 Hoang Sam Str., Nghia Do Wart, Cau Giay Distr., Hanoi City, Vietnam
[3]Hanoi Open University, B101 Nguyen Hien Str., Hai Ba Trung Distr., Hanoi City, Vietnam
[4]Electric Power University, 235 Hoang Quoc Viet Str., North Tu Liem Distr., Hanoi City, Vietnam
[5]Vinh University, 182 Le Duan Str., Vinh City, Vietnam
*Corresponding author: hodinhquangdhv@gmail.com

Received 28 February 2020; revised 15 May 2020; accepted 18 May 2020; posted 19 May 2020 (Doc. ID 391634); published 23 June 2020

In this paper, a thin film of oil red O coated by partial dielectric mirrors (PRFORO) operating as an optical bistable device is proposed. The equation of the output–input intensity relation considering nonlinear absorption inside PRFORO is derived and the optical bistability (OB) of PRFORO is shown. Additionally, the influence of the nonlinear refractive, absorptive coefficients of oil red O (ORO), reflective coefficient of mirrors, and the thickness of thin film on the OB is numerically investigated and discussed. As a result, the threshold switching power is lower than 19 mW; the minimum power of output up-state is larger than 40 μW for the optimal PRFORO designed with an ORO concentration larger than 0.1 mM; the thickness of the thin film is longer than 0.1 mm; and the reflective coefficient of mirrors is lower than 93%. The proposed model is suitable for all-optical switches, optical images, and signal processing.

https://doi.org/10.1364/AO.391634

1. INTRODUCTION

When an optical nonlinear dispersive (or absorptive) medium, whose reflective index (or absorbance) depends on light intensity, due to the nonlinear coefficient n_2 (or nonlinear absorptive coefficient α), is placed in an optical like-cavity system such as Fabry–Perot (FP) [1–4], Mach–Zehnder [5,6], and Michelson interferometers [7,8], or ring cavity [9–11], light is reflected back and forth in the nonlinear medium with different phases that interfere with each other. This can lead to rapid transmission switching and hysteresis. The hysteresis (or bistability) of output light depends on the phase matching of reflected light rays. It means that the transmittance of those systems is a function of the refractive index, which is controlled by the output intensity [12]. Those "so-called" optical bistable devices (OBDs) are used as spatial light modulators [4], optical ultrahigh-speed switches, and image processing [3]. The combination of some bistable devices is realized as logic gates "AND," "OR," and "NOT" [13,14]. When using the conventional nonlinear medium as liquid and gas having the low and positive nonlinearity ($0 < n_2 < 10^{-10}$ cm^2/W), the threshold switching power must be high enough to generate an ON-state (the up-state of output power) [13]. Even when the dichloroethane with a nonlinear refractive coefficient of $n_2 \approx 10^{-7}$ cm^2/W is used to design the nonlinear Fabry–Perot interferometer (NFPI), its threshold switching power could be higher than decades of watts [4]. Moreover, there are disadvantages when using the liquid or gas because it needs the thick medium (a cuvette to hold them must be thick), demanding a big interferometer configuration. Since technological development of the InSb, GaAs, and Te semiconductor bulks [2], GaAs-AlGaAs quantum wells [3], nonlinear ferroelectric [15] and polystyrene nonlinear photonic crystals [16] with a nonlinear refractive coefficient in the range of $n_2 = \mp(10^{-8} \div 10^{-7})$ cm^2/W [17], the threshold switching power of OBD is reduced to hundreds of milliwatts, or even less [3]. Using those solid materials, the OBD can be designed by a thin film (TF) coated with partial dielectric mirrors (PDMs) on its interfaces [15] or with quantum mirrors [18]. Moreover, in previous works, the high nonlinear coefficient ($n_2 \sim 10^{-6}$ cm^2/W) has been found in the electromagnetic-induced transparency (EIT) atomic medium [19], and the all-optical switch (AOS) has been theoretically proposed [9–11,20–22]. Unfortunately, there are disadvantages when using EIT atomic systems for optical integrated circuits (OICs): i) it is necessary to use no fewer than two laser sources with different wavelengths at the same time [10,11]; ii) the density of the atomic medium must be high ($\sim 2.5 \times 10^{11}$ cm^{-3}), so it needs a long atomic vapor cell (7 cm) [11]; and iii) consequently, it must use a ring cavity with long

length and the OBD's size must be in decimeter scale at least, which is similar to that using the Mach–Zehnder interferometer [5]. It could be expected that the OBD as well as the AOS could be used for OICs in the future. Fortunately, recently many organic dyes with the high nonlinear refractive coefficient of $n_2 = \mp(10^{-8} \div 10^{-5})$ cm^2/W (as in semiconductors and the EIT medium) are synthesized and used for laser limiting [23] and AOS [24]. The dried TF of organic dyes as Orange G, Acid Blue 29, and oil red O (ORO) with a thickness below a millimeter is used to design the laser limiter of the detector [25,26], nonlinear optical tweezers [27,28], and nonlinear microscope objective [29]. Previous successes are an opportunity to propose a PRFORO operating as an OBD. Moreover, in almost all previous works [2,4,13,14], the absorption effect in the equation describing the output–input intensities has not yet been considered. So, when using ORO with high nonlinear absorbance, the output property of PRFORO will be investigated at the same time as both nonlinear effects: absorptive and dispersive (Kerr effect) ones. Moreover, the influence of the principle parameter on the output properties that determine the configuration of the OBD has not been investigated yet in detail.

In this paper, we present a proposed model of PRFORO. The equation describing the output–input relation of light intensities considering the nonlinear absorbance are derived. The influence of the ORO concentration, thickness of TF, reflection coefficient of PDMs, and initial phase shift on the output properties are investigated. Finally, discussion of the optimal configuration of PRFORO with low threshold switching power and highest light transport efficiency (LTE) also are shown.

2. MODEL FOR SIMULATION

We consider a TF with thickness d of ORO with nonlinear refractive coefficient n_2 and nonlinear absorption coefficient β [cm/W]. It is coated by PDM, with a reflection coefficient R on its surfaces. The model of PRFORO is illustrated in Fig. 1.

A laser beam with electric amplitude A_0 irradiates into PRFORO at an incident angle α. A part is reflected at angle α, and another one is refracted through the front mirror at angle γ. The reflection, refraction, and transmission amplitudes of laser light (B_i, C_i, D_i, $i = 1, 2, 3 \ldots$ m) through PRFORO are described by ray optics, illustrated in Fig. 2.

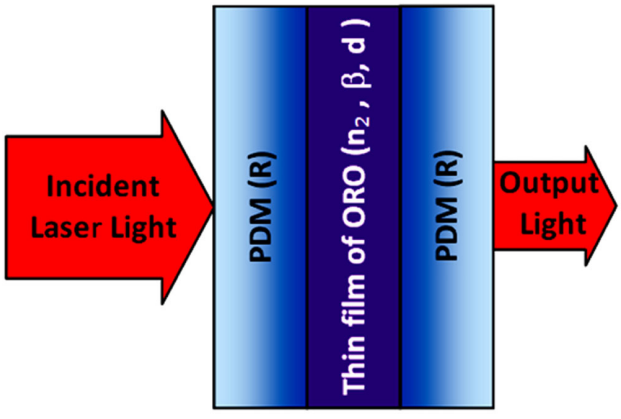

Fig. 1. Simulation model of proposed PRFORO.

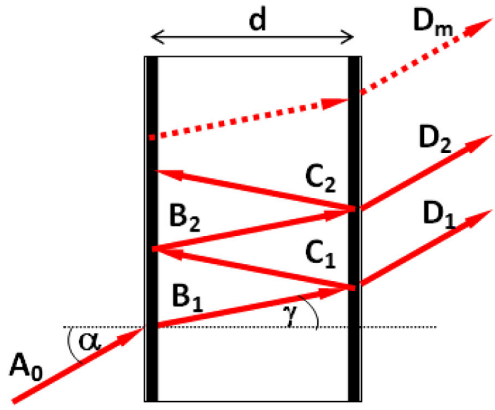

Fig. 2. Optical paths of light through PRFORO.

Using the optical scheme of rays (in Fig. 2), we derive the input–output relation of input and output laser intensities. We consider the approximations that the reflection coefficient of the PDM is high enough so that the intensity of light propagating back and forth inside PRFORO does not change; the input and diffraction angles are small; the linear absorption is negligible (to choose the laser wavelength in the inside high transmission spectrum of ORO), and then the nonlinear absorption and dispersion play the main role.

The electric field of input light E_{in} can be simplified as the following:

$$E_{\text{in}} = A_0 \exp[i(\omega t - kz - \varphi_0)], \tag{1}$$

where $\omega = 2\pi c/\lambda$ is the angle frequency, $k = 2\pi/\lambda$, the wavenumber, λ, the wavelength, c , light velocity, z, position in the propagation direction, and φ_0, the initial phase. The reflection, refraction, and transmission of light continue to be shown in Fig. 2. We have the set of relations of light ray amplitudes,

$$\left.\begin{aligned} |B_1| &= |A_0|\sqrt{1-R} \\ |C_1| &= |B_1|\sqrt{R}e^{-d\beta|B_1|^2} = |A_0|\sqrt{R(1-R)}\,e^{-d\beta|A_0|^2(1-R)} \\ |D_1| &= |B_1|\sqrt{1-R}e^{-d\beta|B_1|^2} = |A_0|\,(1-R)e^{-d\beta|A_0|^2(1-R)} \end{aligned}\right\}, \tag{2}$$

$$\left.\begin{aligned} |B_2| &= |A_0|\,R\sqrt{(1-R)}e^{-d\beta|A_0|^2(1-R)} \\ |C_2| &= |B_2|\sqrt{R} = |A_0|\,R\sqrt{R(1-R)}\,e^{-d\beta|A_0|^2(1-R)} \\ |D_2| &= |B_2|\sqrt{1-R}e^{-d\beta|A_0|^2(1-R)} = |A_0|\,R(1-R)\,e^{-2d\beta|A_0|^2(1-R)} \end{aligned}\right\}. \tag{3}$$

Finally, we have an expression for the mth transmitted ray,

$$|D_m| = |A_0|\,R^{m/2}(1-R)^{m/2}\,e^{-md\beta|A_0|^2(1-R)}. \tag{4}$$

As shown in Ref. [30], the path difference of two neighboring rays is given as

$$\Delta s = 2dn/\sqrt{1-\sin^2\gamma}, \tag{5}$$

where

$$n = n_0 + n_2 I_c = n_0 + n_2|A_0|^2(1-R) \tag{6}$$

is the refractive index of ORO, n_0 is the linear index, and $I_c = (1/2)c|A_0|^2(1-R)$ is the light intensity inside PRFORO. The path difference relating to phase shift [31] is given as the following:

$$\theta = \frac{2\pi \Delta s}{\lambda} + \Delta\varphi, \tag{7}$$

where $\Delta\varphi$ is the phase shift by the initial refraction. Using Eqs. (5)–(7), we have

$$\theta = \frac{4\pi n_2 d|A_0|^2(1-R)}{\lambda\sqrt{1-\sin^2\gamma}} + 2\delta, \tag{8}$$

where

$$2\delta \approx \frac{4\pi n_0 d}{\lambda\sqrt{1-\sin^2\gamma}} + \Delta\varphi \tag{9}$$

is the total initial phase shift, called the cavity phase tuning [32]. In fact, we can choose $\alpha \approx \gamma = 0$, so

$$\theta = \frac{4\pi n_2 d|A_0|^2(1-R)}{\lambda} + 2\delta, \quad 2\delta \approx \frac{4\pi n_0 d}{\lambda} + \Delta\varphi. \tag{10}$$

Then, the output light is the sum of all transmitted rays, i.e., we have

$$I_{\text{out}} = \sum_{i-1}^{m} |D_i|^2 e^{ji\theta}. \tag{11}$$

Substituting Eqs. (4) and (10) into Eq. (11), using relations $I = (1/2)c|A|^2$, $1-\cos\theta = 2\sin^2(\theta/2)$, and with rearrangements, we have the output–input relation of intensities as the following:

$$I_{\text{out}}\left\{1 + \frac{4Re^{-d\beta(1-R)I_{\text{in}}}}{\left(1-Re^{-d\beta(1-R)I_{\text{in}}}\right)^2} \times \sin^2(\phi+\delta)\right\} = \frac{(1-R)^2 e^{-d\beta(1-R)I_{\text{in}}}}{\left(1-Re^{-d\beta(1-R)I_{\text{in}}}\right)^2} I_{\text{in}}, \tag{12}$$

where

$$\phi = \frac{2\pi n_2 d\left(e^{-d\beta(1-R)I_{\text{in}}}-1\right)\left(1+Re^{-d\beta(1-R)I_{\text{in}}}\right)}{\lambda(1-R)} I_{\text{in}}. \tag{13}$$

Using Eq. (12), we will simulate the optical bistability (OB) of PRFORO and influence of parameters as ORO concentration, thickness of TF, and reflection coefficient of PDM, and initial phase shift on threshold switching power (TSP) $P_{\text{th,max}}$ and minimum power of output up-state (MPoS) $P_{\text{out,min}}$. To obtain OB, we choose the first period of the sine function only. We use the following approximation:

$$\sin(\phi+\delta) = \sin(\mp k\pi + \phi + \delta) \equiv \sin\left(\phi' \pm \delta'\right), \tag{14}$$

where $\phi' = \left\lceil \frac{\phi+\delta}{\pi} \right\rceil$ is the remainder of division $\frac{\phi+\delta}{\pi}$, and δ' is the modified phase shift that satisfies the condition, $\delta' \ll \phi' < \pi$.

3. SIMULATION RESULTS AND DISCUSSION

We use the TF of ORO with different concentrations C [mM] in acetonitrile solvent. The nonlinear refractive index (n_2) and nonlinear absorptive (β) coefficients change corresponding to the ORO concentration. As shown in previous work [33], the ORO has a transmission coefficient of about 90% at wavelengths longer 530 nm. The coefficients n_2 and β of ORO at the wavelength of 532 nm are approximately inverse and directly proportional to the concentration C, respectively (see Figs. 3 and 4).

In the evaporating process, the thickness of TF is controlled from $d = 0.18$ mm to $d = 0.26$ mm. We consider PDM having the reflection coefficient $R = (93 \div 97)\%$. The output property of PRFORO is investigated by using the laser beam with wavelength $\lambda = 532$ nm, beam radius $W = 1$ μm , and the average power tuned in the range $P_{\text{in}} = (0 \div 300)$ mW. Using Eqs. (12)–(14), the OB is simulated and presented in Fig. 5.

We can see that with a given collection of parameters, the TSP, $P_{\text{th,max}}$, is about 230 mW and the MPoS, $P_{\text{out,min}}$, is about 480 μW, which means that the LTE is $E_{\text{tran}} = P_{\text{out,min}}/P_{\text{th,max}} = 2.08 \times 10^{-3}$. It is about 10 times higher than that of the NFPI using dichloroethane (see Fig. 6), where $E_{\text{tran}} \approx 1 \times 10^{-4}$ for the case of $n_2 = 1 \times 10^{-7}$ cm^2/W, $d = 2$ mm, and $R = 95\%$; $E_{\text{tran}} \approx 2.5 \times 10^{-4}$ for the case of $n_2 = 1 \times 10^{-7}$ cm^2/W, $d = 10$ mm, and $R = 90\%$. The enhancement of E_{tran} of PRFORO in comparison to NFPI depends mainly on the improvement of the nonlinear refractive coefficient [$|n_2| \sim 10^{-6}$ [cm^2/W] (see Fig. 3) $> n_2 = 10^{-7}$ [cm^2/W] (see Fig. 6)].

Moreover, from the results obtained in previous work [4], shown in Fig. 6, we see E_{tran} depends not only on the nonlinear refractive index coefficient, but also on the thickness of the nonlinear medium and the reflection coefficient R. That means that

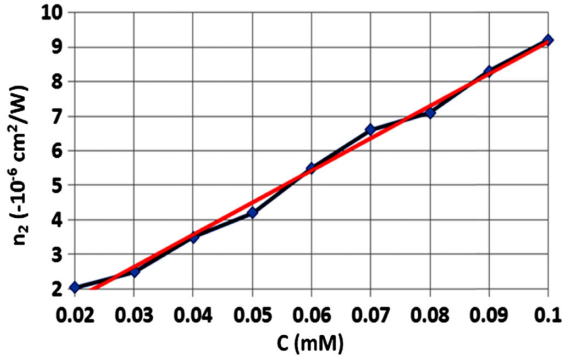

Fig. 3. Nonlinear refractive index coefficient (with minus sign) versus concentration of ORO; experimental data (black) and its trend line (red).

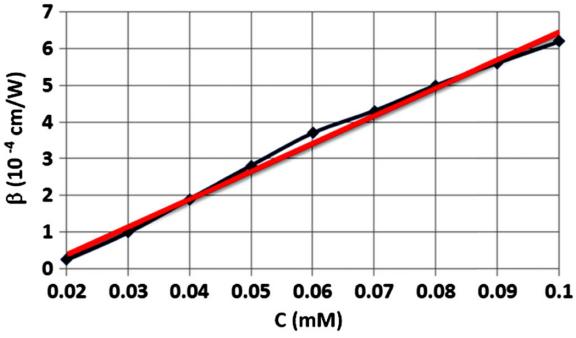

Fig. 4. Nonlinear absorptive coefficient versus concentration of ORO; experimental data (black) and its trend line (red).

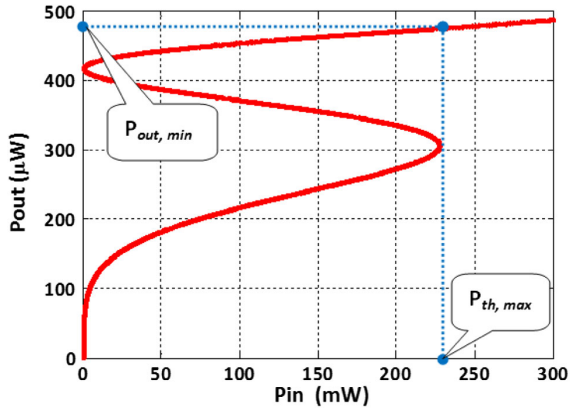

Fig. 5. OB of PRFORO with C = 0.02 [mM], $d = 0.18$ mm, $R = 93\%$, and $\delta' = 0.015\pi$.

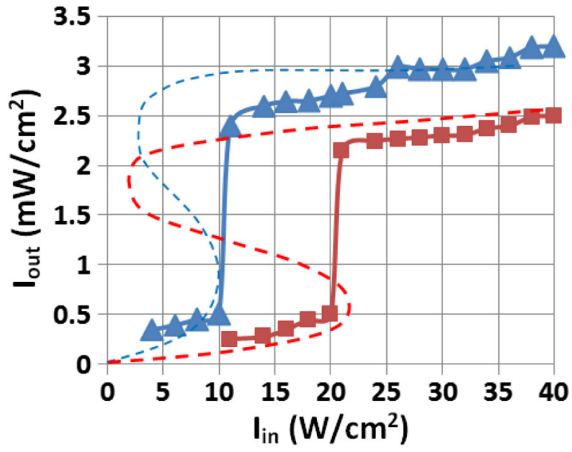

Fig. 6. OB of NFPI using dichloroethane with $n_2 = 1 \times 10^{-7}$ cm^2/W, $d = 10$ mm, $R = 90\%$, (rectangles) and $d = 2$ mm, $R = 95$ % (triangle); theoretical (dashes); experimental (dots) [4].

$P_{\text{th,max}}$ and $P_{\text{out,min}}$ depend on the principal parameters used to design PRFORO. Using data in Figs. 3 and 4, the dependence of $P_{\text{th,max}}$ on the ORO concentration (C[mM]) is presented in Fig. 7. We see $P_{\text{th,max}}$ and $P_{\text{out,min}}$ reduce with the increase of the concentration. The attitudes of the two curves in Fig. 7 are similar; hence, the E_{tran} is nearly constant and equals to 2.08×10^{-3}. Although E_{tran} does not change with the increase of the ORO concentration, the reduction of $P_{\text{th,max}}$ will be of interest. The reduction of $P_{\text{th,max}}$ shows that the higher ORO concentration is, the stronger the nonlinear absorptive and dispersive effects in PRFORO are, corresponding to higher nonlinear absorptive and refractive coefficients (see Figs. 3 and 4).

The above consideration is confirmed by studying the dependence of $P_{\text{out,min}}$ and $P_{\text{th,max}}$ on the thickness of TF (see Fig. 8). From Fig. 8, it is clear that $P_{\text{out,min}}$ and $P_{\text{th,max}}$ reduce with an increase of the thickness d. The LTE, E_{tran}, reduces slightly ($E_{\text{tran}} = (2.08 \div 2.0) \times 10^{-3}$ versus $d = (0.18 \div 0.26)$ mm). So far, we can conclude that the increase of the TF thickness is similar to the increase of the ORO concentration, which causes the increase of both nonlinear absorptive and dispersive effects.

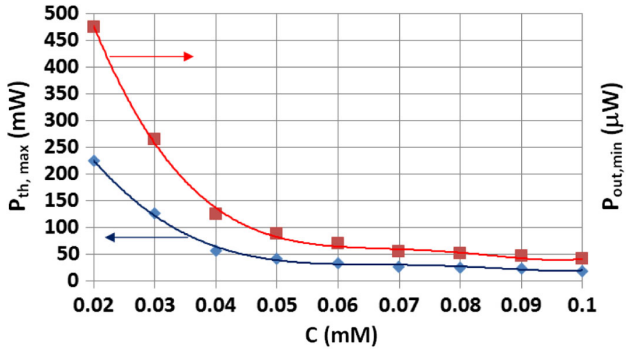

Fig. 7. $P_{\text{th,max}}$ (blue) and $P_{\text{out,min}}$ (red) versus C for the case of $d = 0.18$ mm, $R = 93\%$, $\delta' = 0.015\pi$.

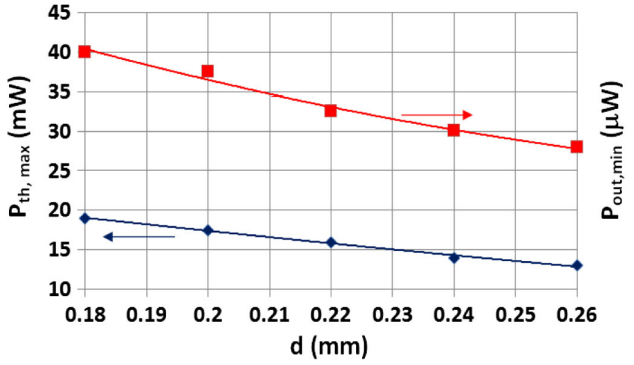

Fig. 8. $P_{\text{th,max}}$ (blue) and $P_{\text{out,min}}$ (red) versus d calculated for the case of $C = 0.1$ [mM], $R = 93\%$, $\delta' = 0.015\pi$.

As shown in Fig. 1 and Eq. (12), the OB depends also on the interference between forward and backward fields inside PRFORO, i.e., it depends on the reflection coefficient R of PDM.

$\delta' = 0.015\pi$, $d = 0.26$ mm, $C = 0.1$ mM are fixed; the OBs of PRFORO with a different value of the reflection coefficient R are simulated and illustrated in Fig. 9. The dependence of $P_{\text{out,min}}$ and $P_{\text{th,max}}$ on R are presented in Fig. 10. We see that as $P_{\text{out,min}}$ decreases and $P_{\text{th,max}}$ increases, E_{tran} decreases powerfully from 2.08×10^{-3} to 0.3×10^{-3} with an increase of R. This behavior can be explained by following reasons: i) increasing of R results in the enhance fields' interference, i.e., the increase of the number of back and forth propagations inside PRFORO; ii) it also causes the fields inside PRFORO and output transmission to be lower; iii) then the reduction of the fields inside PRFORO results in the resonant condition to be unsatisfied; iv) so that P_{in} and the $P_{\text{th,max}}$ must be increased. Finally, the reflection coefficient R of PDM is decreased to increase E_{tran}.

To choose the initial phase shift, accuracy would be a difficult problem in the experiment. Therefore, we have calculated the OB with different initial phase shifts (see Fig. 11). Clearly, we see that the small phase shift does not influence the shape of OB, i.e., and the output property of PRFORO.

From all results obtained above, in order to obtain the optimal PRFORO operating as an OBD with the lowest TSP ($P_{\text{th,max}} \leq 19$ mW) and the highest LTE, ($E_{\text{tran}} \geq 2 \times 10^{-3}$),

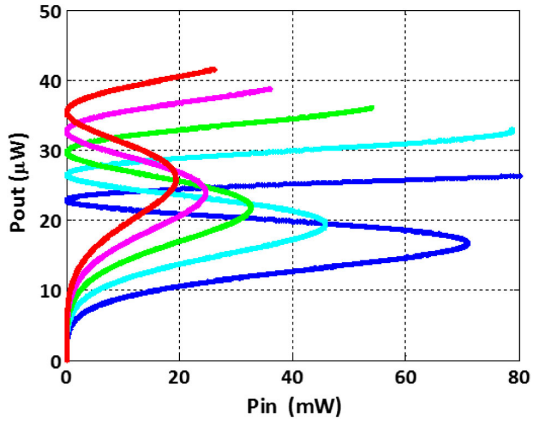

Fig. 9. OB of PRFORO with $C = 0.1$ mM, $\delta' = 0.015\pi$, $d = 0.26$ mm, and $R = 93\%$ (red); $R = 94\%$ (magenta); $R = 95\%$ (green); $R = 96\%$ (cyan); $R = 97\%$ (blue).

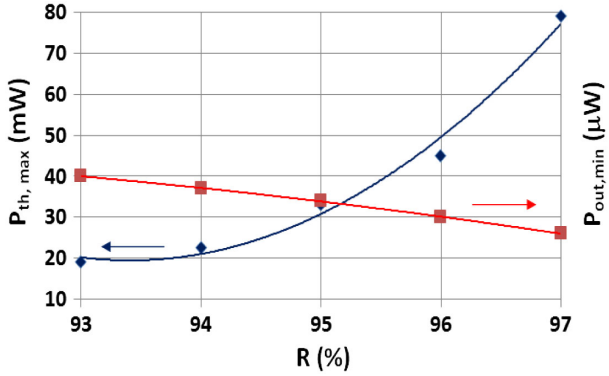

Fig. 10. $P_{\text{th,max}}$ (blue) and $P_{\text{out,min}}$ (red) versus R calculated for the cases of $C = 0.1$ mM, $\delta' = 0.015\pi$, $d = 0.26$ mm.

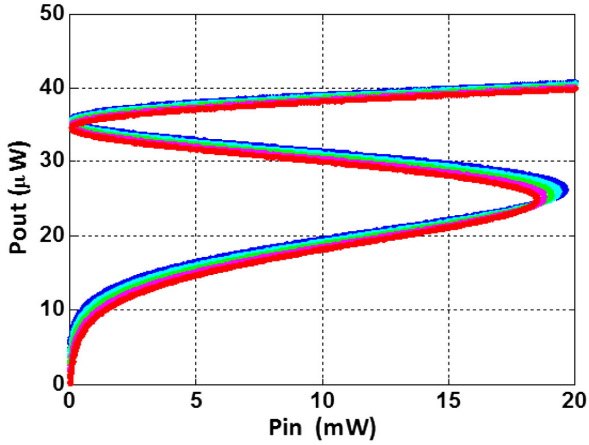

Fig. 11. $P_{\text{th,max}}$ (blue) and $P_{\text{out,min}}$ (red) versus δ' changing from 0.015π (red) to 0.065π (blue) calculated for the cases of $C = 0.1$ mM, $R = 93\%$, $d = 0.26$ mm.

it is necessary to choose the parameters as follows: the concentration of $C \geq 0.1$ mM, the thickness of TF, $d \geq 0.26$ mm, and the reflection coefficient of PDM of $R \leq 93\%$. It can operate as an OBD used to design an AOS, an optical image, and signal processors. The PRFORO proposed could be used for a laser beam's redistribution, and NFPI has been investigated [4] (see Fig. 12).

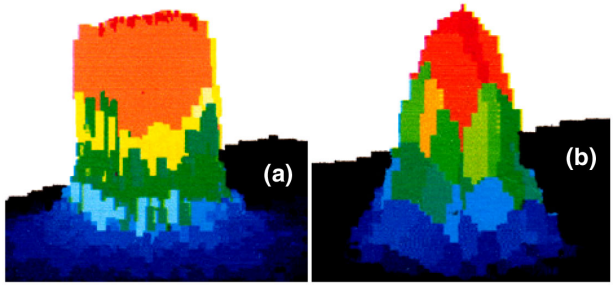

Fig. 12. Spatial redistribution (a) of laser Gaussian beam (b) by NFPI [4].

4. CONCLUSION

The partial reflection coated TF of ORO with high nonlinear absorptive and refractive coefficients operating as the OBD is proposed. The output–input relation of intensities concerning the nonlinear absorptive effect is derived and the OB simulated. We have investigated the influence of the main parameters as the concentration of ORO in acetonitrile solvent, thickness of TF, and the reflection coefficient of partial dielectric coated mirrors on the OB, especially on the threshold switching power and MPoS. The obtained result is the optimal collection of parameters to design an OBD with a lower threshold switching power and high LTE. Moreover, our model is easy to design: the OBD's size is on the millimeter scale, much smaller than that using an EIT medium. This would provide an incentive to experimental investigation for all-optical switching, optical images, and signal processing.

Disclosures. The authors declare no conflicts of interest.

REFERENCES

1. E. Garmire, "Signal processing with a nonlinear Fabry-Perot," Proc. SPIE **0269**, 69–74 (1981).
2. E. Abraham and S. D. Smith, "Nonlinear Fabry-Perot interferometers," J. Phys. E **15**, 33–39 (1982).
3. E. Garmire, "Resonant optical nonlinearities in semiconductors," IEEE J. Sel. Top. Quantum Electron. **6**, 1094–1110 (2000).
4. N. V. Hoa, H. Q. Quy, and V. N. Sau, "Experimental investigation bistability and spatial redistribution of laser beam of Fabry-Perot interferometer embedded diclor-ethane pumped by Nd:YAG laser," Commun. Phys. **15**, 223–228 (2005).
5. H. Q. Quy, V. N. Sau, and N. V. Hoa, "Catastrophe characters of the unsymmetrical Mach-Zehnder interferometer with absorption-nonlinear material," Commun. Phys. **13**, 157–164 (2003).
6. Q. Q. Ho, N. S. Vu, V. H. Nguyen, and T. T. T. Nguyen, "Optical bistability effect of two-port nonlinear fiber Mach-Zehnder interferometers," Commun. Phys. **21**, 161–168 (2011).
7. H. Q. Quy, N. V. Hoa, and V. N. Sau, "Bistability of close nonlinear Michelson interferometer," in *Sixth German-Vietnam Seminar (GVS6) Physics and Engineering*, Chemnitz, Germany (2003), pp. 144–147.
8. N. V. Hoa, H. Q. Quy, and V. N. Sau, "Close Michelson interferometer semi-embedded by nonlinear medium for laser beam redistributing," in *Seventh German-Vietnam Seminar (GVS7) Physics and Engineering*, Halong, Germany (2005), pp. 166–170.

9. J. Yuan, W. Feng, P. Li, X. Zhang, Y. Zhang, H. Zheng, and Y. Zhang, "Controllable vacuum Rabi splitting and optical bistability of multi-wave-mixing signal inside a ring cavity," Phys. Rev. A **86**, 063820 (2012).
10. Z. Zhang, H. Chen, L. Zhang, D. Zhang, X. Li, Y. Zhang, and Y. Zhang, "Unveiling the relationship between optical bistability and vacuum Rabi splitting," Europhys. Lett. **117**, 53001 (2017).
11. Z. Zhang, D. Ma, J. Liu, Y. Sun, L. Cheng, G. A. Khan, and Y. Zhang, "Comparison between optical bistabilities versus power and frequency in a composite cavity-atom system," Opt. Express **25**, 8916–8925 (2017).
12. B. E. A. Saleh and M. C. Teich, *Fundamentals of Photonics*, J. W. Goodman, ed. (Wiley, 2012), p. 848.
13. Y. Okabayashi, T. Isoshima, E. Nameda, S.-J. Kim, and M. Hara, "Two-dimensional nonlinear Fabry-Perot interferometer: an unconventional computing substrate for maze exploration and logic gate operation international," J. Nanotechnol. Mol. Comput. **3**, 13–23 (2011).
14. Y. Liu, J. Wang, S. Le, and W. Lin, "Output property of a nonlinear Fabry-Perot interferometer," Proc. SPIE **2229**, 210–216 (1994).
15. A.-B. M. A. Ibrahim, D. R. Tilley, and J. Osman, "Optical bistability from ferroelectric Fabry-Perot interferometer," J. Ferroelectr. **355**, 140–144 (2007).
16. Y. Liu, F. Qin, Z.-Y. Wei, Q.-B. Meng, D.-Z. Zhang, and Z.-Y. Li, "10 fs ultrafast all-optical switching in polystyrene nonlinear photonics crystals," Appl. Phys. Lett. **95**, 131116 (2009).
17. E. Garmire and A. Kost, *Nonlinear Optics in Semiconductors I* (Academic, 1998), p. 27.
18. F. Fratini, E. Mascarenhas, L. Safari, J.-Ph. Poizat, D. Valente, A. Auffèves, D. Gerace, and M.-F. Santos, "Fabry-Perot interferometer with quantum mirrors: nonlinear light transport and rectification," Phys. Rev. Lett. **115**, 149901 (2015).
19. D. X. Khoa, L. V. Doai, P. V. Trong, T. M. Cuong, V. N. Sau, N. H. Bang, and L. N. M. Anh, "EIT enhanced self-Kerr nonlinearity in the three-level lambda system under Doppler broadening," Commun. Phys. **24**, 217–224 (2014).
20. H. R. Hamedi, "Optical switching, bistability and pulse propagation in five-level quantum schemes," Laser Phys. **27**, 066002 (2017).
21. H. Jafarzadeh, "All-optical switching in an open V-type atomic system," Laser Phys. **27**, 025204 (2017).
22. H. M. Dong, L. T. Y. Nga, and N. H. Bang, "Optical switching and bistability in a degenerated two-level atomic medium under an external magnetic field," Appl. Opt. **58**, 4192–4199 (2019).
23. S. Jeyaram and T. Geethakrishnan, "Third-order nonlinear optical properties of acid green 25 dye by Z-scan method," Opt. Laser Technol. **89**, 179–185 (2017).
24. H. A. Badran, R. C. Adul-Hail, H. S. Shaker, and Q. M. Hassan, "An all-optical switch and third-order optical nonlinearity of 3,4-pyridinediamine," Appl. Phys. **B123**, 31 (2018).
25. L. T. Nguyen, N. T. Hong, C. T. B. Thi, and A. Q. Le, "The numerical methods for analyzing the Z-scan data," J. Nonlinear Opt. Phys. Mater. **23**, 1450020 (2014).
26. K. R. Rekha and A. Ramalingam, "Nonlinear characteristics and optical limiting effect of oil Red O azo dye in liquid and solid media," J. Mod. Opt. **56**, 1096–1102 (2009).
27. H. Q. Quy, T. D. Thanh, D. Q. Tuan, and N. M. Thang, "Nonlinear optical tweezers for longitudinal control of dielectric particles," Opt. Commun. **421**, 94–98 (2018).
28. N. M. Thang, H. Q. Quy, T. D. Thanh, D. Q. Tuan, D. T. Viet, and D. Q. Khoa, "3D control stretched length of lambda–phage WLC DNA molecule by nonlinear optical tweezers," Opt. Quantum Electron. **52**, 51 (2020).
29. Q. H. Quang, T. T. Doan, T. D. Quoc, V. D. Thanh, K. B. Thanh, L. L. Nguyen, and T. N. Manh, "Nonlinear microscope objective using thin layer of organic dye for optical tweezers," Eur. J. Phys. D **74**, 52 (2020).
30. L. V. Taracov, *Laser Physics* (MIR, 1980).
31. V. Degiorgio, "Phase shift between transmitted and reflected optical fields of a semi-reflecting lossless mirror is $\pi/2$," Am. J. Phys. **48**, 81–82 (1980).
32. W. Demtroder, *Laser Spectroscopy* (Springer, 1982).
33. N. T. Lam, "Investigating third order nonlinear optical properties of organic dyes by nonlinear refractive index and nonlinear absorption index and application," Ph.D. dissertation (Ho Chi Minh City University of Science, 2018).